Distance limits to intermediate- and high-velocity clouds

Smoker, J., Fox, A., & Keenan, F. (2011). Distance limits to intermediate- and high-velocity clouds. *Monthly Notices of the Royal Astronomical Society*, *415*, 1105-1118. https://doi.org/10.1111/j.1365-2966.2011.18647.x

Published in:
Monthly Notices of the Royal Astronomical Society

Document Version:
Publisher's PDF, also known as Version of record

Monthly Notices
of the
ROYAL ASTRONOMICAL SOCIETY

Mon. Not. R. Astron. Soc. **415,** 1105–1118 (2011) doi:10.1111/j.1365-2966.2011.18647.x

Distance limits to intermediate- and high-velocity clouds⋆

J. V. Smoker,[1]† A. J. Fox[1] and F. P. Keenan[2]

[1]*European Southern Observatory, Alonso de Cordova 3107, Casilla 19001, Vitacura, Santiago 19, Chile*
[2]*Astrophysics Research Centre, Department of Physics and Astronomy, Queen's University Belfast, Belfast BT7 1NN*

Accepted 2011 March 4. Received 2011 March 4; in original form 2010 October 17

ABSTRACT

We present optical spectra of 403 stars and quasi-stellar objects in order to obtain distance limits towards intermediate- and high-velocity clouds (IHVCs), including new Fibre-fed Extended Range Optical Spectrograph (FEROS) observations plus archival ELODIE, FEROS, High Resolution Echelle Spectrometer (HIRES) and Ultraviolet and Visual Echelle Spectrograph (UVES) data. The non-detection of Ca II K interstellar (IS) absorption at a velocity of -130 to $-60\,\mathrm{km\,s^{-1}}$ towards HDE 248894 ($d \sim 3$ kpc) and HDE 256725 ($d \sim 8$ kpc) in data at signal-to-noise ratio (S/N) > 450 provides a new firm lower distance limit of 8 kpc for the anti-centre shell HVC. Similarly, the non-detection of Ca II K IS absorption towards HD 86248 at S/N ~ 500 places a lower distance limit of 7.6 kpc for Complex EP, unsurprising since this feature is probably related to the Magellanic System. The lack of detection of Na I D at S/N $=$ 35 towards Mrk 595 puts an improved upper limit for the Na I column density of $\log(N_{\mathrm{NaD}} <) 10.95\,\mathrm{cm^{-2}}$ towards this part of the Cohen Stream where Ca II was detected by Wakker et al. Absorption at $\sim -40\,\mathrm{km\,s^{-1}}$ is detected in Na I D towards the Galactic star PG 0039+049 at S/N $= 75$, placing a firm upper distance limit of 1 kpc for the intermediate-velocity cloud south (IVS), where a tentative detection had previously been obtained by Centurión et al. Ca II K and Na I D absorption is detected at $-53\,\mathrm{km\,s^{-1}}$ towards HD 93521, which confirms the upper distance limit of 2.4 kpc for part of the IV arch complex obtained using the *International Ultraviolet Explorer* (*IUE*) data by Danly. Towards HD 216411 in Complex H a non-detection in Na D towards gas with $\log(N_{\mathrm{H\,I}}) = 20.69\,\mathrm{cm^{-2}}$ puts a lower distance limit of 6.6 kpc towards this HVC complex. Additionally, Na I D absorption is detected at $-43.7\,\mathrm{km\,s^{-1}}$ in the star HD 218915 at a distance of 5.0 kpc in gas in the same region of the sky as Complex H. Finally, the Na I/Ca II and Ca II/H I ratios of the current sample are found to lie in the range observed for previous studies of IHVCs.

Key words: stars: early-type – ISM: abundances – ISM: clouds – ISM: general – ISM: structure.

1 INTRODUCTION

Although nearly 50 yr have passed since their discovery (Muller, Oort & Raimond 1963), knowledge of the distance and metallicities of high-velocity clouds (HVCs) remains frustratingly poor. HVCs are defined as interstellar clouds orbiting with velocities incompatible with Galactic rotation; in practice, this means $|v_{\mathrm{LSR}}| >$ 90–100 $\mathrm{km\,s^{-1}}$ at high Galactic latitudes. Clouds with 40–50 $< |v_{\mathrm{LSR}}| <$ 90–100 $\mathrm{km\,s^{-1}}$ are referred to as intermediate-velocity clouds (IVCs). HVCs and IVCs are important tools for studying Galactic evolution, since they trace the various interactions between the Milky Way and the surrounding intergalactic medium (IGM), including the accretion of low-metallicity gas and the outflow of metal-enriched gas (see the review by Wakker & van Woerden 1997). To date, an upper distance limit to only a handful of intermediate- and high-velocity clouds (IHVCs) has been obtained, although recently progress has been made in ascribing a Galactic origin to at least some of the clouds, including Complex A (van Woerden et al. 1999), Complex WB (Thom et al. 2006), Complex C (Wakker et al. 2007; Thom et al. 2008), and the Cohen Stream, Complex GCP and Complex g1 (Wakker et al. 2008). That said, some compact HVCs *may* lie at extragalactic distances (Braun & Burton 1999). However, recent detections of HVC analogues around nearby galaxies such as M 31 and M 33 (Westmeier, Braun & Thilker 2005; Westmeier, Brüns & Kerp 2008; Putman et al. 2009), coupled with non-detections of HVCs in external galaxy groups (Pisano et al. 2004), lend strong support to the Galactic origin although some

⋆Based on European Southern Observatory (ESO) programme IDs 078.C-0493(A) and 171.D-0237(B).

†E-mail: jsmoker@eso.org

observations are still consistent with the idea that a fraction of HVCs could be minihaloes in the outskirts of the Local Group (Giovanelli et al. 2010).

In the present paper, we determine distance limits and metallicities for a handful of IHVCs using echelle spectroscopy of background stars and quasi-stellar objects (QSOs). The motivation for the current research is to provide distances to IHVCs in order to discriminate between various formation mechanisms including the remnants of cold dark matter (Moore et al. 1999) which predicts HVCs of distances of several hundreds of kpc or a 'circumgalactic' population with distances of tens of kpc (Westmeier et al. 2007, and references therein).

Our paper is laid out as follows. Section 2 describes the sample and observations of IHVCs. Included is a table noting the cases where the current sightlines cross the known IHVC complexes, and a description of the observations and data reduction for the optical spectra. Section 3 gives the main results, including the derivation of column densities or their upper/lower limits for the optical transitions studied in the local gas and HVC sightlines, and shows the optical and H I spectra. Section 4 presents the discussion, including the derivation of improved lower distance limits towards three IHVCs and a brief discussion concerning the Routly–Spitzer (RS) effect in these clouds and an attempt to derive their physical conditions. Finally, Section 5 gives a summary of the main findings and suggestions for future work.

2 THE SAMPLE, OBSERVATIONS AND DATA REDUCTION

We use a combination of new observations and data from various astronomical archives. The species considered in this paper are shown in Table 1.

2.1 New observations and archival data used for distance limit determinations to IHVCs

In order to maximize the number of IHVC sightlines studied, we used a combination of new observations plus data from a number of astronomical archives as described below.

2.1.1 New observations with FEROS

The Fibre-fed Extended Range Optical Spectrograph (FEROS; Kaufer et al. 1999) sample of objects includes sightlines towards one IVC [the intermediate-velocity cloud south (IVS); Centurión et al 1994], two classical HVCs [the Cohen Stream: van Kuilenburg 1972; Hulsbosch 1978; Tamanaha 1995, and the anti-centre shell (ACS); Tamanaha 1996, and references therein] and one extreme positive velocity cloud (Complex EP; Wakker & van Woerden 1991) that may be related to the Magellanic Stream. Four of the sightlines are towards early-type stars, with the final sightline towards a Seyfert galaxy lying behind the Cohen Stream.

Table 1. Main transitions studied in this paper. Wavelengths and oscillator strengths are from Morton (2003, 2004). Column 4 gives the ionization potential (IP) in eV. For comparison the IP of H I is 13.60 eV.

Transitions	λ_{air} (Å)	f-value	IP (eV)
Ti II	3383.759	0.358	13.58
Ca II	3933.661	0.627	11.87
Na I	5889.951	0.641	5.14
Na I	5895.924	0.320	5.14
K I	7698.965	0.333	4.34

The FEROS observations were taken on the nights of 2006 December 8 and 9. FEROS covers the spectral range ∼3500–9200 Å at a spectral resolution ($\lambda/\Delta\lambda$) of ∼48 000 or ∼6.3 km s^{-1}.

FEROS exposure times were typically 30–50 min, and multiple exposures were taken to facilitate the removal of cosmic rays. Observations of a few fast-rotating B-type stars were taken as telluric standards. The data were reduced using the FEROS pipeline (in MIDAS). A total of 35 flat-fields were used to create the master flat, and the wavelength calibrations taken before the observations started each night were used to define the wavelength solution. Reduction was undertaken using both standard and optimum extractions, with and without cosmic ray removal, respectively. Agreement was found to be good between the two methods. To check the quality of the results, the equivalent widths and velocities of a few lines were compared with previous UVES observations of a few B-type stars taken from the online version of the Paranal Observatory Project (POP) survey (Bagnulo et al. 2003). Agreement was found to be within 1 km s^{-1} in velocity for one compared sightline and within 5 per cent in the equivalent widths of strong lines for two compared sightlines.

The individual FEROS spectra were co-added using SCOMBINE within IRAF,[1] converted into American Standard Code for Information Interchange (ASCII) format and then read into DIPSO for further analysis. Initially, this included shifting to the kinematical local standard of rest (LSR) using corrections generated by the program RV (Wallace & Clayton 1996), then normalizing the spectra by fitting polynomials of type $y = a0 + a1 \times x + a2 \times x^2 + a3 \times x^3 + \cdots$ to the stellar continuum in the region of interest. Typical orders were between 3 and 5. The errors in the fitting were not included in the analysis. The normalization procedure gives the signal-to-noise ratio (S/N) in the final spectra by considering the rms scatter of the data about the fit. We note that these S/N values are rather high and do not include systematic contributions to the error budget. They may therefore be overoptimistic.

For the regions around Na I D and K I ($\lambda = 7698$ Å), telluric spectra were removed as described in Smoker et al. (2006).

Table 2 shows the five objects observed using FEROS. Columns 1–4 list the object name, Galactic coordinates and apparent V-band magnitude. Columns 5 and 6 give the distance and distance above or below the Galactic plane of the target, and column 7 gives the IHVC complex name. Finally, columns 8–11 give the total integration time in hours and S/N per resolution element of the extracted spectra around the wavelengths of Ca II K, Na I D and K I. Equivalent widths, velocity centroids and full width at half-maximum (FWHM) velocity values of the optical transitions were obtained by fitting Gaussians to the normalized spectra using the ELF package within DIPSO (Howarth et al. 2003). These results were used as initial inputs to the VAPID code (Howarth et al. 2002) which performs a curve-of-growth analysis to provide the final values of the column densities and their associated errors.

2.1.2 FEROS and UVES data from the ESO archive

FEROS observations of five bright target stars towards the Cohen Stream and Complex WE were extracted from the European

[1] IRAF is distributed by the National Optical Astronomy Observatories, USA.

Table 2. The sample observed with FEROS in 2006 December. Mrk 595 is at $z = 0.0272$ or a distance of ∼109 Mpc assuming $H_0 = 74.2\,\mathrm{km\,s^{-1}\,Mpc^{-1}}$ (Riess et al. 2009). The S/N values are given per resolution element. See Section 2.1.1 for details.

Object	l (°)	b (°)	m_v (mag)	d_* (pc)	z (pc)	IHVC name	Time (h)	S/N Ca II K	S/N Na I D	S/N K I
PG 0039+049	118.59	−57.64	12.91	1050[a]	890	IVS, MS	2.5	60	75	50
Mrk 595	164.76	−46.55	14.7	–	–	CS	5.7	5	35	30
HDE 248894	187.89	−2.51	9.29	3000[b]	130	ACS	1.5	500	600	350
HDE 256725	192.31	+3.36	10.44	8000[c]	470	ACS	2.0	450	600	350
HD 86248	264.59	+18.11	9.56	7600[b]	2360	EP	1.5	500	500	300

Reference codes: ACS – anti-centre shell; CS – Cohen Stream; IVS – intermediate-velocity cloud south; EP – extreme positive velocity cloud; MS – Magellanic Stream.
[a]Centurión et al. (1994); [b]Wakker (2001); [c]Garmany, Conti & Massey (1987).

Southern Observatory (ESO) archive. Their reduction was performed in the same manner as for the main sample, using calibrations taken either the day before or the day after the observation. Observations were extracted for a further 143 targets (a mixture of QSOs, Galactic stars and pulsars) observed with the UVES echelle spectrometer (Dekker et al. 2000) mounted on the 8.2-m Kueyen unit of the Very Large Telescope. Many of these sightlines lie in 'holes' in the IHVC complexes. Some of the data were reduced with the UVES pipeline (in MIDAS) using average extraction for the high-S/N data and optimal extraction for the intermediate- or low-S/N data. The remaining spectra are the reduced versions from the ESO archive which became available online during the progress of this work.

2.1.3 Sightlines from the ELODIE archive

Reduced ELODIE spectra of 237 targets (mostly bright stars) were retrieved from the online ELODIE archive (Moultaka et al. 2004), corrected to the kinematical LSR using RV and corrected for telluric absorption. These data were taken using the 1.93-m telescope of Observatoire de Haute Provence between 1993 and 2006, have a spectral resolution of ∼42 000 and span the wavelength region ∼4000–6800 Å, covering the Na I D lines but unfortunately not Ca II K.

2.1.4 HIRES data from the Keck archive

HIRES observations of 13 targets (a mix of Galactic stars and QSOs) were taken from the Keck Observatory Archive. A description of HIRES may be found in Vogt et al. (1994). The data were reduced using standard methods in IRAF which included bias subtraction, flat-fielding and wavelength calibration, before co-adding using SCOMBINE and correction to the kinematical LSR. Only Ca II K was reduced, apart from PHL 957 where we examined both Ca II and Na I D. The spectral resolutions of the data are typically ∼40 000.

2.1.5 21-cm data from the LAB survey

For the H I 21-cm spectra, we adopt data from either (i) the Effelsberg 100-m radio telescope, which has a spatial resolution of 9 arcmin, with column densities, velocities and velocity widths of the H I components from fig. 1 of Wakker et al. (2001) or (ii) the Southern Villa-Elisa H I Survey data (Bajaja et al. 2005), corrected for the effects of stray radiation or (iii) the Leiden–Dwingeloo Survey, for sightlines with Dec. $> -20°$ (Hartmann & Burton 1997). The latter two surveys have been merged to form the Leiden/Argentine/Bonn (LAB) H I line survey (Kalberla et al. 2005), which has a velocity resolution of $1\,\mathrm{km\,s^{-1}}$ and brightness temperature sensitivity of 0.07 K.

3 RESULTS

In this section we present the main results from the new observations and archive data. A subsample of the ELODIE, FEROS, HIRES and UVES archival data are shown in Table 3, with the whole sample being available online. Table 4 lists the archive subsample that has produced new results, as well as the new FEROS observations. IHVCs are listed alphabetically.

3.1 Spectra towards IHVCs

Fig. 1 shows the optical and H I 21-cm LAB survey spectra for sightlines where new FEROS observations were taken, plus towards sightlines discussed in Section 4.2. In the cases where there was a stellar line present, often this was removed during the normalization process and a 'No*' comment included in the figure panel. Fig. A1 (available online – see Supporting Information) shows the same type of spectra as Fig. 1, but for *all* of the archive-extracted ELODIE, FEROS, HIRES and UVES spectra as well as the LAB H I spectra. Table 4 presents optical and H I information on the IHVCs only, excluding the Galactic and Large Magellanic Cloud (LMC)

Table 3. A subsample of the ELODIE, FEROS, HIRES and UVES objects. The complete table is available online – see Supporting Information.

Object	l (°)	b (°)	m_b (mag)	m_v (mag)	SpecType	d_* (pc)	IHVC	Inst.	R	Species	S/N
HE 0121−2826	0.00	0.00	15.89	15.53	DA	–		UVES	20 000	Ca II	35
MOA 2002-blg12	1.93	−3.62	–	–		–		UVES	40 000	Na I	10
HD 1638	4.29	−82.68	10.11	8.78	K1.0 III	–		UVES	40 000	Ca II	100
CS 22948−104	5.32	−51.42	14.55	13.96		–		UVES	40 000	Ca II	60
HE 2242−3621	6.50	−62.62	–	–		–		UVES	20 000	Ca II	30
WD 1708−147	7.66	14.85	–	14.50		–	K	UVES	33 000	Ca II	60
HE 2351−3207	8.72	−77.13	–	–		–		UVES	20 000	Ca II	13

Table 4. IHVC sightlines. For metal-line detections, the observed column density is given; for non-detections, a 5σ upper limit to the column density is given. See text for details.

Object	l, b (°)	Dist. (pc)	IHVC name	$v_{\rm H\,I}$ (km s^{-1})	$N_{\rm H\,I}$ (cm^{-2})	H I dat	Opt. spec.	S/N	$v_{\rm Opt}$ (km s^{-1})	$N_{\rm Opt}$ (cm^{-2})	$N_{\rm Opt}^{\rm Pred}$ (cm^{-2})
HDE 248894	187.89, −2.51	3000	ACS	−56.0 ± 0.0	19.60 ± 0.00	W01	Ca K	500	–	<9.98	11.76
HDE 248894	187.89, −2.51	3000	ACS	−40.0 ± 0.0	19.47 ± 0.00	W01	Ca K	500	–	<9.98	11.73
HDE 248894	187.89, −2.51	3000	ACS	−56.0 ± 0.0	19.60 ± 0.00	W01	Na D	600	–	<9.72	11.46
HDE 248894	187.89, −2.51	3000	ACS	−40.0 ± 0.0	19.47 ± 0.00	W01	Na D	600	–	<9.72	11.35
HD 256725	192.31, 3.36	8000	ACS	−61.0 ± 0.0	19.52 ± 0.00	W01	Ca K	450	–	<10.03	11.74
HD 256725	192.31, 3.36	8000	ACS	−61.0 ± 0.0	19.52 ± 0.00	W01	Na D	600	–	<9.72	11.40
BD+28 3137	59.94, 11.53	1202	C	−124.6 ± 0.8	19.70 ± 0.02	LAB	Ca K	210	–	<10.37	11.78
Mrk 595	164.76, −46.55	QSO	CS	124.0 ± 0.0	19.42 ± 0.00	W01	Na D	35	–	<10.95	11.31
HD 86248	264.59, 18.11	7600	EP	201.0 ± 0.0	18.88 ± 0.00	W01	Ca K	100	–	<10.68	11.60
HD 83312	284.77, −10.68	690	EP	79.5 ± 0.8	20.15 ± 0.02	LAB	Ti II	200	–	<10.46	11.34
HD 83312	284.77, −10.68	690	EP	79.5 ± 0.8	20.15 ± 0.02	LAB	Ca K	270	–	<10.03	11.88
HD 216411	108.03, −0.35	6600	H	−97.4 ± 2.0	20.69 ± 0.02	LSB	Na D	230	–	<10.19	12.37
HD 216411	108.03, −0.35	6600	H	−96.5 ± 2.0	20.39 ± 0.02	LAB	Na D	230	–	<10.19	12.08
HE 0929-0424	238.52, 32.78	–	HVC	147.8 ± 0.7	19.36 ± 0.00	LAB	Ca K	40	–	<11.16	11.71
HD 125632	99.05, 58.02	103	IVA	−43.2 ± 0.1	19.68 ± 0.01	LAB	Na D	200	–	<10.25	11.53
HD 109387	125.22, 47.26	140	IVA	−49.0 ± 0.2	19.97 ± 0.01	LAB	Na D	400	–	<9.95	11.78
HD 109247	128.65, 62.13	200	IVA	−56.5 ± 0.2	19.78 ± 0.01	LAB	Na D	80	–	<10.65	11.61
HD 106591	132.57, 59.42	31	IVA	−56.8 ± 0.3	19.87 ± 0.07	LAB	Na D	250	–	<10.15	11.69
HD 99747	138.87, 52.73	33	IVA	−54.0 ± 0.2	19.67 ± 0.01	LAB	Na D	130	–	<10.44	11.52
HD 103287	140.84, 61.38	27	IVA	−57.2 ± 0.1	19.80 ± 0.01	LAB	Na D	250	–	<10.15	11.63
J1208+485	140.91, 66.63	QSO	IVA	−54.0 ± 2.0	19.60 ± 0.03	LAB	Na D	100	–	<10.55	11.47
DG LEO	210.95, 48.37	160	IVA	−41.1 ± 0.2	19.87 ± 0.01	LAB	Na D	150	–	<10.38	11.69
HD 87015	211.17, 51.48	485	IVA	−41.0 ± 3.0	19.80 ± 0.02	W01	Na D	170	–	<10.26	11.63
HD 92825	213.52, 60.84	63	IVA	−32.0 ± 1.0	20.03 ± 0.01	LAB	Na D	230	–	<10.13	11.82
HD 89021	175.87, 55.08	41	IVA	−51.7 ± 0.1	19.80 ± 0.01	W01	Na D	250	–	<10.15	11.63
HD 93521	183.14, 62.15	2409	IVA	−54.1 ± 0.2	19.70 ± 0.01	W01	Ca K	150	−56.4 ± 2.0	12.20 ± 0.40	11.55
HD 93521	183.14, 62.15	2409	IVA	−54.1 ± 0.2	19.70 ± 0.01	W01	Na D	150	−56.0 ± 2.0	10.65 ± 0.10	11.55
HD 122008	21.00, 74.21	650	IVC	−23.0 ± 3.0	19.65 ± 0.02	LAB	Na D	80	−28.6 ± 1.0	10.90 ± 0.20	11.50
BD+28 3137	59.94, 11.53	1202	IVC	−74.8 ± 3.0	20.14 ± 0.01	LAB	Ca K	210	–	<10.37	11.88
HD 43378	155.59, 19.12	45	IVC	−84.5 ± 2.0	19.77 ± 0.03	LAB	Na D	350	–	<10.01	11.60
HD 43378	155.59, 19.12	45	IVC	−48.0 ± 2.0	19.85 ± 0.02	LAB	Na D	350	–	<10.01	11.67
HD 71066	284.82, −79.82	147	IVC	−36.1 ± 0.1	20.31 ± 0.00	LAB	Ca K	230	–	–	11.92
HD 100546	296.37, −8.73	218	IVC	95.8 ± 0.2	19.92 ± 0.01	LAB	Ca K	220	–	<10.02	11.83
HE 1316-1834	312.04, 44.40	–	IVC	27.7 ± 1.0	19.48 ± 0.04	LAB	Ca K	20	–	–	11.74
HD 116706	11.48, 81.73	93	IVC?	−22.1 ± 0.1	19.81 ± 0.01	LAB	Na D	250	−18.2 ± 1.0	10.65 ± 0.30	11.64
HD 218915	108.06, −6.89	5000	IVC?	−50.6 ± 0.8	20.76 ± 0.02	LAB	Na D	140	−43.7 ± 1.0	11.92 ± 0.05	12.43
HD 218915	108.06, −6.89	5000	IVC?	−43.8 ± 0.2	20.57 ± 0.02	LAB	Na D	140	−43.7 ± 1.0	11.92 ± 0.05	12.28
HD 219989	105.20, −17.95	270	IVSou	−29.0 ± 3.0	20.19 ± 0.01	LAB	Na D	160	–	<10.29	11.96
PG 0039+049	118.59, −57.64	1050	IVSou	−51.0 ± 0.0	19.64 ± 0.00	W01	Ca K	60	–	<10.90	11.77
PG 0039+049	118.59, −57.64	1050	IVSou	−51.0 ± 0.0	19.64 ± 0.00	W01	Na D	75	–	<10.62	11.50
PG 0039+049	118.59, −57.64	1050	IVSou	−51.0 ± 0.0	19.64 ± 0.00	W01	K I	50	–	<10.96	–
HD 6116	125.24, −21.48	105	IVSou	−55.6 ± 0.1	19.99 ± 0.01	LAB	Na D	220	–	<10.21	11.79
QSO 0105+1619	128.69, −46.35	–	IVSou	−62.3 ± 1.1	19.75 ± 0.01	W01	Ca K	40	−67.0 ± 3.0	12.05 ± 0.10	11.79
QSO 0105+1619	128.69, −46.35	–	IVSou	−62.3 ± 1.1	19.75 ± 0.01	W01	Na D	20	−63.0 ± 3.0	>13.60	11.60
HD 9531	132.32, −24.85	154	IVSou	−44.0 ± 3.0	19.98 ± 0.01	LAB	Na D	250	–	<10.15	11.79
HD 12174	137.15, −21.42	411	IVSou	−47.0 ± 4.0	19.58 ± 0.17	LAB	Na D	90	−37.7 ± 1.0	10.70 ± 0.10	11.44
HD 12174	137.15, −21.42	411	IVSou	−33.5 ± 4.0	19.96 ± 0.15	LAB	Na D	90	−23.0 ± 1.0	11.20 ± 0.10	11.76
HD 24398	162.29, −16.69	300	IVSou	−49.0 ± 0.3	19.64 ± 0.04	LAB	Na D	300	–	<10.07	11.50
HD 107966	221.04, 83.85	75	IVSp	−35.1 ± 0.2	20.03 ± 0.00	LAB	Na D	200	−32 ± 1	–	11.83
HD 107935	223.16, 83.74	86	IVSp	−35.0 ± 0.1	20.09 ± 0.00	LAB	Na D	250	–	<10.15	11.88
HD 97603	224.23, 66.83	20	IVSp	−39.3 ± 0.2	19.85 ± 0.00	LAB	Na D	280	–	<10.10	11.67
HD 89021	175.87, 55.08	41	M	−106.9 ± 0.7	19.28 ± 0.02	LAB	Na D	300	–	<10.07	11.19
PG 0039+049	118.59, −57.64	1050	MS	−367.0 ± 0.0	19.44 ± 0.00	W01	Ca K	60	–	<10.90	11.73
PG 0039+049	118.59, −57.64	1050	MS	−367.0 ± 0.0	19.44 ± 0.00	W01	Na D	75	–	<10.62	11.33
PG 0039+049	118.59, −57.64	1050	MS	−367.0 ± 0.0	19.44 ± 0.00	W01	K I	50	–	<10.96	–
HD 152478	336.78, −5.42	230	WE	−141.6 ± 0.0	19.08 ± 0.03	LAB	Ca K	100	–	<10.20	11.65
HD 152478	336.78, −5.42	230	WE	−124.1 ± 0.0	19.84 ± 0.00	LAB	Na D	900	–	<9.54	11.67

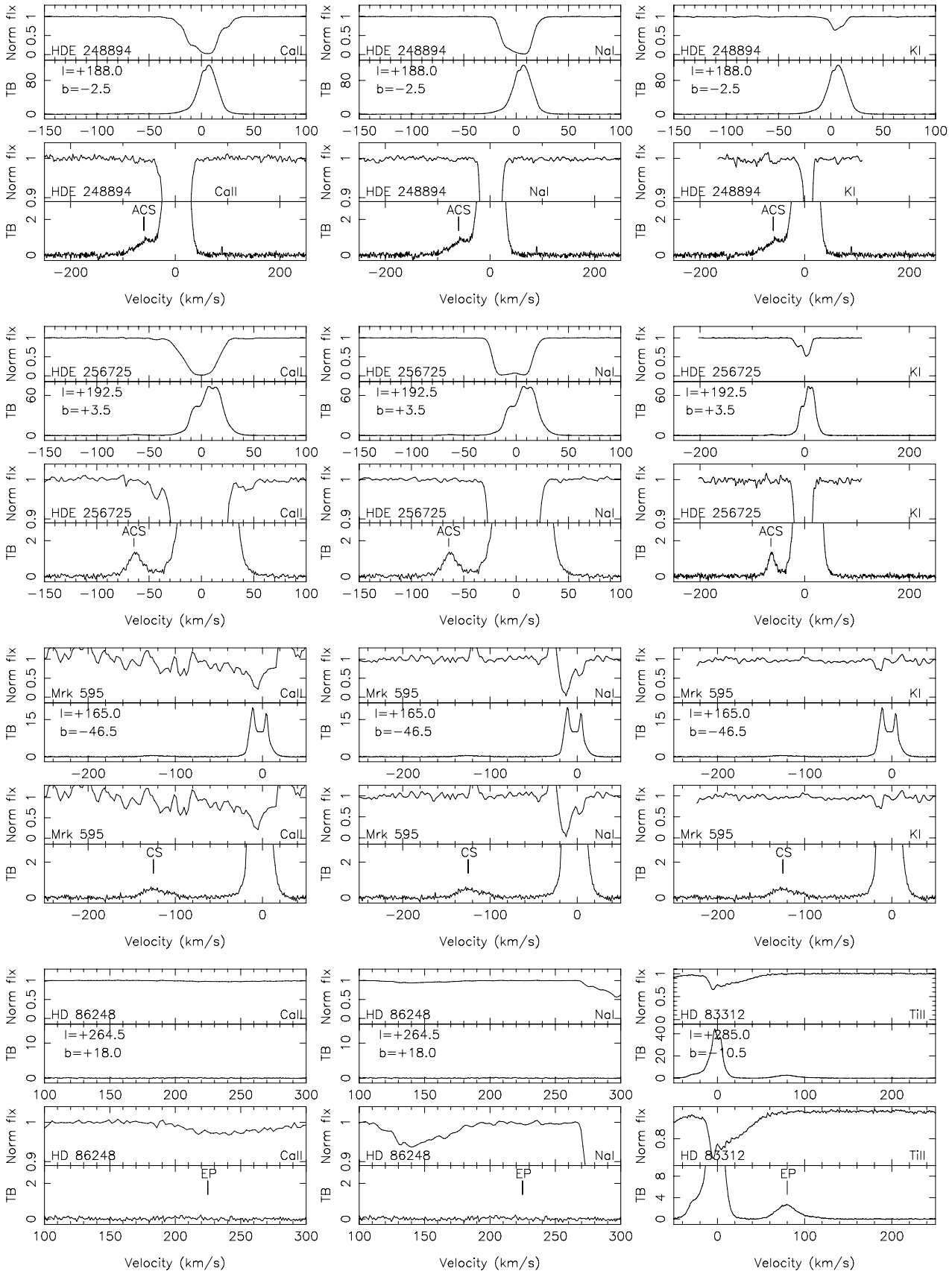

Figure 1. Optical Ti II, Ca II K, Na I D and K I normalized spectra and 21-cm H I LAB survey spectra towards the new FEROS sample, plus towards archival sightlines discussed in the text. The ordering is by IHVC name. See Section 2.1.1 for details.

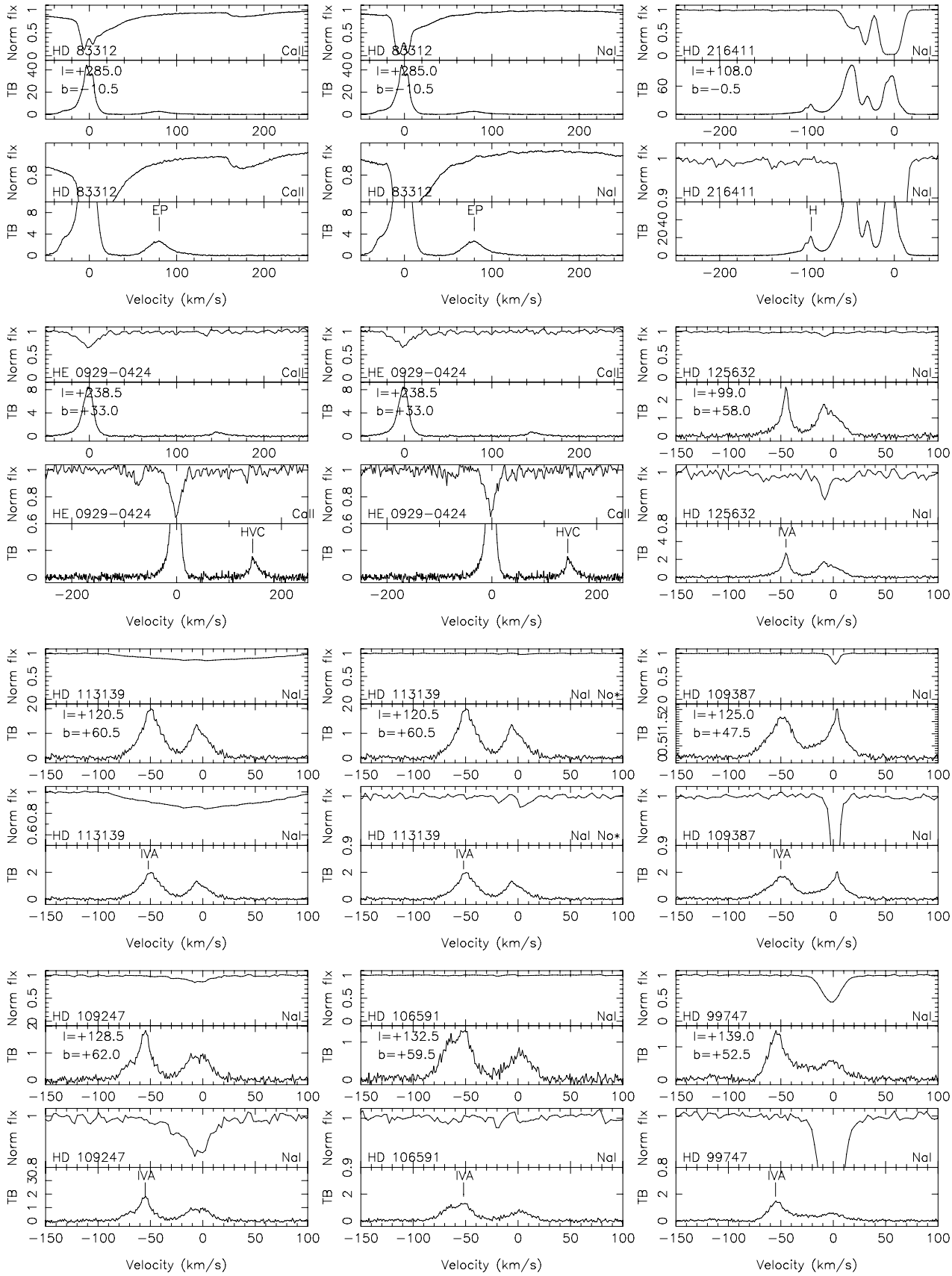

Figure 1 – *continued*

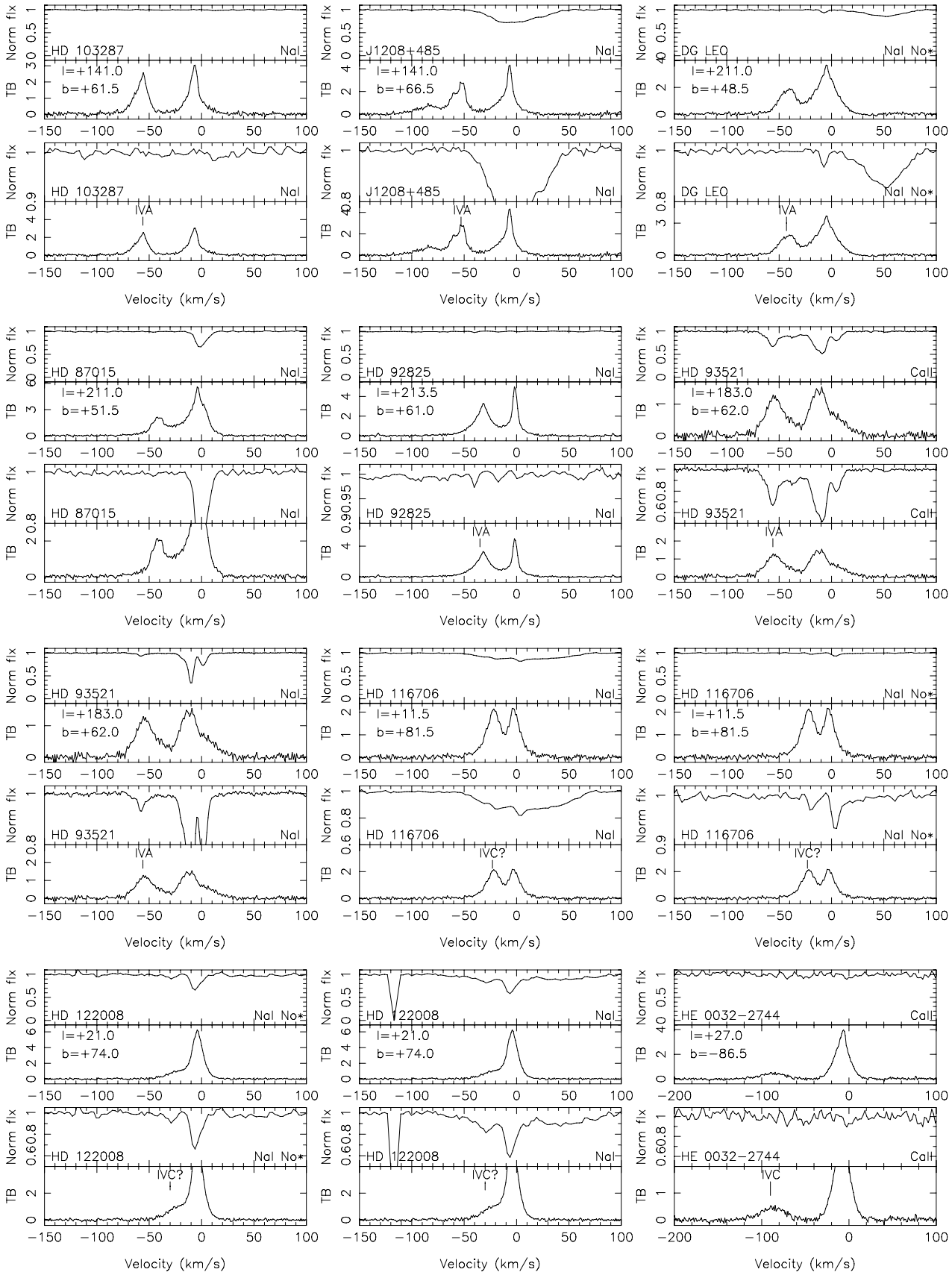

Figure 1 – *continued*

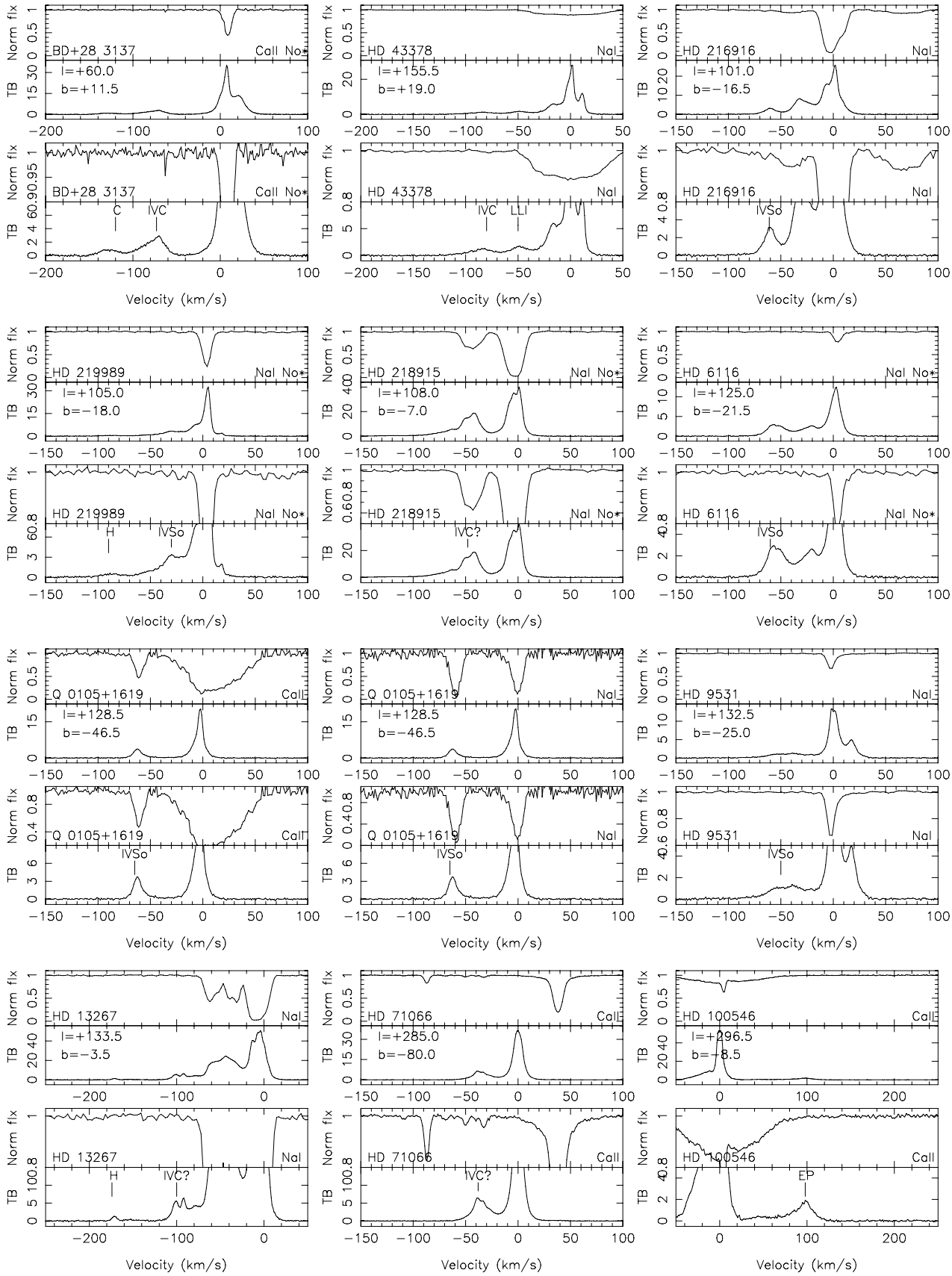

Figure 1 – *continued*

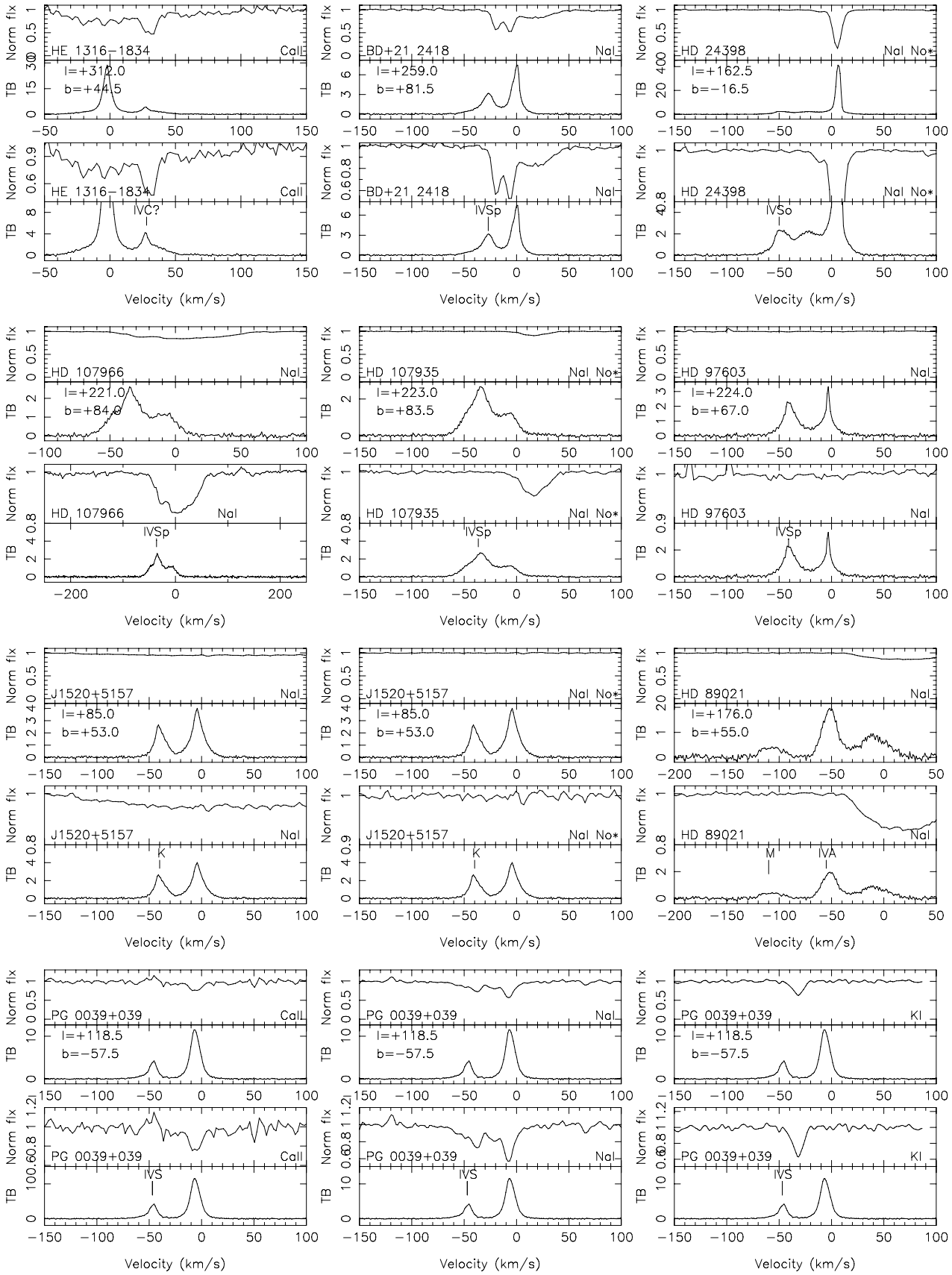

Figure 1 – *continued*

components. We note that although the 21-cm H I spectra in Figs 1 and A1 are taken from the LAB survey with a 0.°5 beam, the H I results in Table 4 are derived either from the LAB survey or from H I profiles obtained with the Effelsberg telescope (W01) which has a spatial resolution of 9 arcmin at this wavelength. The rms noise levels for the Effelsberg H I spectra are 0.08 K for PG 0039+049, 0.04 K for Mrk 595, 0.06 K for both HDE 248894 and HD 256725 and 0.08 K for the LAB spectra of HD 86248.

4 DISCUSSION

In this section we present improved distance limits towards a handful of IHVCs, discuss the RS effect on Na I/Ca II as well as Ca I/H I ratios in the objects detected as well as the physical conditions in the clouds.

4.1 Distances to IHVCs: methodology

The method of estimating distances to IHVCs is discussed fully in Schwarz, Wakker & van Woerden (1995). For an upper distance limit, the detection of non-circumstellar optical absorption in the spectrum of a target star at known distance is sufficient. Lower distance limits can only be set if no optical absorption is seen at a sufficient S/N, the abundance of the optical element is known (generally from observations of the same part of the complex towards QSOs) and the H I column density (from which the predicted metal column density is estimated) is accurately defined using a pencil beam. As a general rule in the optical domain, lower distance limits are only thought meaningful if derived from Ti II or Ca II data whose transitions show much less variability in their abundance patterns than do Na I or K I (Wakker & Mathis 2000; Smoker et al. 2003; Hunter et al. 2006).

In the following we define the metallicity of Ca II as

$$\left[\frac{\mathrm{Ca\,II}}{\mathrm{H\,I}}\right] = [\log N(\mathrm{Ca\,II}) - \log N(\mathrm{H\,I})] - \left[\frac{\mathrm{Ca}}{\mathrm{H}}\right]_{\odot}, \quad (1)$$

where $[\mathrm{Ca/H}]_{\odot} = -5.65$ is the solar Ca abundance taken from Morton (2003).

To determine whether a non-detection of an IHVC is meaningful as a lower distance limit, the following method was used. We first estimate the 5σ limiting equivalent width of a feature for element X that would have been detected if the cloud were in front of the stellar probe, viz.

$$\mathrm{EW_{lim}}(X) = 5(\mathrm{S/N})^{-1}_{\mathrm{cont}}\Delta\lambda_{\mathrm{instr}}, \quad (2)$$

this equation only being valid in the case where the feature is unresolved, where $(\mathrm{S/N})_{\mathrm{cont}}$ is the S/N per resolution element ($\Delta\lambda_{\mathrm{instr}}$) in the continuum. Once this limiting equivalent width was estimated, it was used to determine the limiting column density N_{lim}, assuming the lines lie on the linear part of the curve of growth, viz.

$$N_{\mathrm{lim}} = 1.13 \times 10^{20}\frac{\mathrm{EW_{lim}}}{\lambda^2 f}, \quad (3)$$

where λ is the wavelength in Å and f is the oscillator strength of the line being investigated. Finally, we predict the optical column density that would be expected from the observed H I value, using

$$\log A_{\mathrm{p}}^{\mathrm{WM00}}(\mathrm{Ti}) = [-0.69 \times (\log N_{\mathrm{H\,I}} - 19.50)] - 8.36, \quad (4)$$

$$\log A_{\mathrm{p}}^{\mathrm{WM00}}(\mathrm{Ca}) = [-0.78 \times (\log N_{\mathrm{H\,I}} - 19.50)] - 7.76, \quad (5)$$

$$\log A_{\mathrm{p}}^{\mathrm{WM00}}(\mathrm{Na}) = [-0.16 \times (\log N_{\mathrm{H\,I}} - 19.50)] - 8.12, \quad (6)$$

which are taken from Wakker & Mathis (2000) and where $\log A$ refers to the gas-phase abundance relative to H I, viz. $\log A = \log N_{\mathrm{opt}} - \log H_{\mathrm{H\,I}}$. After comparing the observed and predicted column densities, the rms dispersions for Ti, Ca and Na were found to be 0.39, 0.42 and 0.52 dex, respectively, and thus there is a large scatter (particularly for Na I) in the column densities and gas-phase abundances for similar clouds. We note that using the above relationships only gives an approximate estimation of the real abundances because (1) the H I column density is derived from a large beam and does not take fine-scale structure into account: Savage et al. (2000) find that $N(\mathrm{H\,I})(\mathrm{Ly}\alpha) = 0.6\text{–}1.0 \times N\ (\mathrm{H\,I})(21\ \mathrm{cm})$, i.e. the 21-cm column density tends to overestimate the true H I column density along a pencil-beam sightline; (2) the intrinsic Ti/H or Ca/H ratio varies somewhat from cloud to cloud; (3) the Ti/H or Ca/H ratio may vary within clouds; (4) we have made no ionization corrections and (5) the H I 21-cm column density is integrated to infinity, whereas the optical metal lines are only measured up to the distance of the stellar probe.

For the non-detections towards IHVCs we use the formulation of appendix 15 of Wakker (2001) in order to determine if a non-detection can be interpreted as being due to the cloud being further away than the probe. For this we assume a factor of 2 in variation caused by H I small-scale structure, factors of 1.5 (Ca II) and 2.5 (Na I) to account for variations in depletion and further factors of 2 (Ca II) and 6 (Na I) for ionization variations. We multiply the above values to obtain a 'safety factor' of 0.8 dex for Ca II and 1.5 dex for Na I. If the column density predicted from H I minus the upper limit to the column density estimated from the spectrum is larger than the safety factor, we ascribe a non-detection as being caused by the cloud being further away from the stellar probe.

4.2 Distance limits and estimated abundances of individual complexes

Some of the current sightlines intersect known IHVC complexes and show absorption components agreeing with the H I IHVC velocities (Wakker 2001). In particular, an upper limit abundance towards one HVC (the Cohen Stream in Na I D) and one IVC (IVS in Ca II K) have been determined, and lower distance estimates towards three IHVCs are obtained (anti-centre HVC, Complex EP and Complex H). Table 4 summarizes these cases. Columns 1–7 list the target name, Galactic coordinates, stellar distance, IHVC complex, observed H I velocity, corresponding log of the H I column density and data source [LAB for Kalberla et al. (2005) and W01 for Wakker et al. (2001)]. Columns 8–9 give the optical species studied and the corresponding S/N. Finally, columns 10–12 list the velocity of any IHVC optical detection, the observed column density or upper limit derived using equations (1)– (3) and the predicted optical species column density derived using equations (4)–(6). In this table we use lower limits only if the difference in the column density predicted from the H I and upper limit to the column density lies outside of the safety factor calculated above. The measured IHVC Na I D column densities are typically ∼0.5 dex lower than the best-fitting value obtained by Wakker & Mathis (2000), with a range from +0.26 dex higher to −0.99 dex lower. Looking in detail at the composite fig. 1 of Wakker & Mathis (2001), the current data points are in better agreement with Ferlet, Vidal-Madjar & Gry (1985) than the IVC data taken from Wakker et al. (2000). However, the scatter in the Na I D measurements is 0.52 dex, so we do not draw any definite conclusions from the difference measured. The offset measured is in contrast to the Ca II K abundance values for low-velocity gas

Table 5. Summary of new IHVC distance limits and confirmation of earlier work. See Section 4.2 for details.

Cloud.	Probe D_l	(l, b) (D_l)	D_l (pc)	Probe (D_u)	(l, b) (D_u)	D_u (pc)
ACS	HD 256725	192.31, 3.36	8000[a]	–	–	–
EP	HD 86248	264.59, 18.11	7600[a]	–	–	–
IVA	HD 87015	211.17, 51.48	400[a]	HD 93521	183.14, 62.15	2400[b]
H	HD 216411	108.03, −0.35	6000[a]	–		–
H	PG 1255+547		870[c]	HD 93521	183.14, 62.15	2400[c]
M	HD 89021	175.87, 55.08	41[a]	–	–	–
IVC	HD 71066	284.82, −79.82	150[a]	–	–	–
IVC	HD 100546	296.37, −8.73	200[a]	–	–	–
IVC	HD 218915	108.06, −6.89	5000[a]	HD 218915	108.06, −6.89	–
IVS	HD 24398	162.29, −16.69	300[a]	PG 0039+049	162.29, −16.69	1050[a,d]
WE	HD 152478	336.78, −5.42	230[a]	HD 156359[e]		12 800[e]

[a]This paper; [b]Danly (1989); [c]Kuntz & Danly (1996); [d]Centurion et al.; [e]Sembach et al (1991).

measured by Smoker et al. (2003) that were found to be 0.5 dex *higher* than the Wakker & Mathis (2000) values.

Table 5 shows a summary of new distance limits and confirmations of existing work. In this table we only include gas with absolute values of LSR velocity of greater than 30 km s^{-1}. Interesting distance limits are discussed below.

4.2.1 *Intermediate velocity cloud south*

IVS is a group of IVCs extending over much of the southern sky and depicted in fig. 17 of Wakker (2001), with velocities between −85 and −45 km s^{-1}. Smoker et al. (2007) use the lack of detected absorption in the Ca II K spectrum of HD 19445 to provide an uninteresting lower distance limit of 39 pc towards this part of the complex.

One of our FEROS sample stars (PG 0039+049) lies towards this IVC, and we obtain S/N values of 60, 75 and 50 in Ca II K, Na I D and K I, respectively, at a spectral resolution of 6.3 km s^{-1}. These sensitivities are somewhat higher than S/N = 40 measured by Centurión et al. (1994) in Na I D in their spectrum of resolution ∼25 km s^{-1}. Centurión et al. (1994) detected absorption in the line wing, which is also detected in the current Na I D spectra. Hence, the present data suggest that this part of IVS lies at a distance of less than 1050 pc.

Towards four other IVS sightlines (HD 219989, HD 6116, HD 9531 and HD 24398), no Na I is seen, with 5σ limits ranging from $\log(N_{\rm Na\,I}) < 10.07$ to $<10.29\,{\rm cm}^{-2}$, compared with the predicted column densities of 11.50–11.96. These lie just on the limit of the 'safety factor' derived in Section 4.1 to provide weak lower distance limits ∼200 pc towards the IVC.

4.2.2 *Anti-centre shell HVC*

The ACS HVC was identified by Heiles (1984) and is depicted in fig. 8 of Wakker (2001). Wide-field H I imaging of the region by Tamanaha (1994, 1997) showed that it contains a 'wealth of filamentary structure' at negative velocities. The shell lies at velocities of −130 to −60 km s^{-1} and $(l, b) \sim (185^\circ, 0^\circ)$. Tamanaha (1996) determined a lower distance limit of ∼610 pc towards AC0 although no other observation currently exists (Wakker 2001). Although Smoker et al. (2007) give a lower distance limit of 2.7 kpc, based on the lack of Ca II K absorption observed at S/N = 610 towards HD 30677, this sightline lies towards feature Anti-centre shell II (ACII), which may not be associated with the ACS. Two of our FEROS targets lie towards the ACS complex: HDE 248894, at a distance of 3.0 kpc (Wakker 2001) and HDE 256725, at a distance of 8.0 kpc (Garmany et al. 1987). Both objects were previously observed by Kulkarni & Mathieu (1986) at a spectral resolution of 10 km s^{-1} and a S/N = 20. Kulkarni & Mathieu (1986) give a predicted Ca II K equivalent width of 105 mÅ, which they estimated assuming a fixed Ca II/H I ratio of −7.89. This is close to the value that would be derived using equation (5), hence our 5σ limit to the equivalent width of 0.8 mÅ appears to set a firm lower distance limit of 8 kpc for this complex.

4.2.3 *Complex EP*

EP is an acronym for the extreme positive velocity clouds (Wakker & van Woerden 1991) seen in fig. 10 of Wakker (2001) and lying at LSR velocities exceeding ∼200 km s^{-1} in a large (115° × 95°) roundish region centred on $(l, b) \sim (270^\circ, 10^\circ)$. In particular, WW 211 is part of the leading arm of the Magellanic Stream and has been observed by Danly, Albert & Kuntz (1993) who obtained a Si II non-detection towards HD 86248. However, their non-detection is not thought by Wakker (2001) to be significant, as the Stream's Si abundance is a factor of ≈4 lower than the standard halo value. Towards HD 86248 the H I column density at a velocity of +201 km s^{-1} is $7.6 \pm 3.0 \times 10^{18}\,{\rm cm}^{-2}$. The star is listed by Wakker et al. (2001) as having a distance of 7.6 ± 1.7 kpc although *Hipparcos* measures an uncertain parallax of 1.84 ± 1.22 mas, corresponding to only 540 pc. We recalculated the distance estimate to this star using spectroscopic parallax equations given in Diplas & Savage (1994). Absolute magnitudes have been estimated from the spectral type, and these estimates are based on the data from Schmidt-Kaler (1982) and have random errors of around 25 per cent. Reddenings have been estimated using the observed $(B - V)$ colour in combination with the colours and spectral types from stars taken from Wegner (1994). We note that the absolute magnitudes from Schmidt-Kaler (1982) are systematically fainter than that in Wegner (2000), although they show better agreement with the estimates from Vacca, Garmany & Shull (1996). Our estimated distance is ∼10 ± 2.5 kpc using Schmidt-Kaler (1982), which puts the star much further away than the uncertain *Hipparcos* parallax. The current FEROS observations are at a S/N = ∼100 in Ca II K and Na I D. The difference in observed and predicted Ca II column density of 0.92 dex exceeds the safety factor for Ca II K of 0.8 dex; hence, lack of interstellar absorption at high velocities at such a S/N seems to place a lower distance of 7.6 ± 1.7 kpc to this part of the complex.

Although an improvement on previous work, the new distance limit derived here cannot confirm either a Galactic or Magellanic origin for this cloud.

4.2.4 The intermediate-velocity arch

The intermediate-velocity arch (IVA) is a large northern set of clouds with $b > 30^{\circ}$, first studied by Wesselius & Fejes (1973). It was mapped in H I at low resolution by Kuntz & Danly (1996) who also derived a distance bracket of 0.9–1.7 kpc.

Of the 14 stellar sightlines towards the IVA, only one shows a detection of Na I. Specifically, towards HD 93521 at $(l, b) = (183\overset{\circ}{.}14, +62\overset{\circ}{.}15)$ we detect corresponding Na I absorption in the IVC component at $-54.1\,\mathrm{km\,s^{-1}}$ with $\log(N_{\mathrm{H\,I}}) = 19.70\,\mathrm{cm^{-2}}$ and $\log(N_{\mathrm{Na\,I}}) = 10.65\,\mathrm{cm^{-2}}$. The feature is seen in both the 5889 and 5895 lines and confirms the upper distance limit of ∼2.4 kpc for this part of the complex determined by the use of *IUE* spectra of resolution $25\,\mathrm{km\,s^{-1}}$ (Danly 1989). All the other 13 sightlines show non-detections, with 5σ upper limits ranging from $\log(N_{\mathrm{Na\,I}}) < 9.95$ to $<10.65\,\mathrm{cm^{-2}}$. Only one of these sightlines [HD 92825 at $(l, b) = (213\overset{\circ}{.}52, +60\overset{\circ}{.}84)$] has a sufficient safety factor to set a weak lower limit of 63 pc to the complex.

4.2.5 The Complex H HVC

Many of our sightlines are in the region of the sky containing Complex H, a group of negative-velocity HVCs centred upon $(l, b) \sim (130^{\circ}, 0^{\circ})$ with velocities from ∼−80 to $-210\,\mathrm{km\,s^{-1}}$. Previous work on this object (Centurión et al. 1994; Smoker et al. 2006) have indicated a distance limit of >4 kpc for the complex.

For the current sightlines, towards HD 216411 at $(l, b) = (108\overset{\circ}{.}03, 0\overset{\circ}{.}35)$ there is no Na I D detected in the spectrum, with S/N = 230 in the HVC at $\sim -100\,\mathrm{km\,s^{-1}}$. The optical non-detection sets a 5σ limit of $\log(N_{\mathrm{Na\,I}}) < 10.19\,\mathrm{cm^{-2}}$ towards this star of distance 6.6 kpc. The H I column density at this position in the sky is $\log(N_{\mathrm{H\,I}}) = 20.69\,\mathrm{cm^{-2}}$; hence, the non-detection appears significant and provide an improved lower distance limit of 6.6 kpc for this complex. The H I mass of this HVC thus exceeds $\sim 1.5 \times 10^6\,\mathrm{M_{\odot}}$.

Blitz et al. (1999) suggested a likely extragalactic origin for Complex H, stating that it is close to the plane, and that *if* it were closer than 40 kpc, the interaction of high-velocity (HV) and Galactic gas would produce some visible signature such as increased Hα X-ray emission that is not visible. An alternative theory was put forward by Lockman (2003), who postulated that Complex H is a satellite of the Milky Way in a retrograde orbit with a distance of 33 ± 9 kpc. Milky Way/HVC interactions have been postulated for other HVCs (Lockman et al. 2008; McClure-Griffiths et al. 2008), and are thought to be necessary to explain Galactic chemical evolution models (e.g. Romano et al. 2006, and references therein). Concerning Complex H, Buenrostro, Lockman & Beckman (2008) *do* detect evidence in H I for a shock front at the leading surface of the HV gas, plus a gas tail that they explain as being caused by its collision with the halo of the Galaxy. The current observations put a lower distance limit for Complex H of ∼6.6 kpc, or distance from the Galactic Centre exceeding ∼15 kpc, hence unfortunately cannot differentiate between the various theories for the cloud's origins.

4.3 Low- and intermediate-velocity gas towards Complex H

Towards the low Galactic latitude object HD 218915 $(l, b) = (108\overset{\circ}{.}06, -6\overset{\circ}{.}89)$, $D = 5.0$ kpc (Savage & Wakker 2009), H I is detected at -50.6 ± 0.8 and $-43.8 \pm 0.2\,\mathrm{m\,s^{-1}}$, with $\log(N_{\mathrm{H\,I}}) = 20.76\,\mathrm{cm^{-2}}$ and $20.57\,\mathrm{cm^{-2}}$. In the Na I D spectrum there is a corresponding detection at $-43.7 \pm 1.0\,\mathrm{km\,s^{-1}}$, with $\log(N_{\mathrm{Na\,I}}) = 11.92\,\mathrm{cm^{-2}}$, thus putting an upper limit of 5 kpc towards this parcel of gas. We note that the relationship between the gas at $-43\,\mathrm{km\,s^{-1}}$ towards HD 218915 and the HVC Complex H (if any) is not clear. At the Galactic longitude and latitude of the probe star, the intermediate-velocity gas is explained by normal Galactic rotation (cf. fig. 1 of Wakker 1991). Hence, whether this gas is a part of the disc of the Galaxy or a part of infalling material is uncertain. It would be useful to map this part of the sky with the many available probes in order to investigate both corotating and HV gas.

4.4 The Routly–Spitzer effect and Na I/Ca II ratio

More than 50 yr ago, Routly & Spitzer (1952) presented evidence that the column density ratio of N(Na I) to N(Ca II) decreases markedly with increasing LSR velocity, in particular, on average, Na I being more abundant in low-velocity clouds than Ca II, with the reverse being true in higher velocity objects. The variation in the N(Na I)/N(Ca II) ratio spans more than four orders of magnitude from ≈0.1 to ≈1000. A similar effect was also seen in the work of Siluk & Silk (1974) who furthermore found that low values of N(Na I)/N(Ca II) are associated with large peculiar values relative to the LSR, proposing also that the majority of the HV components seen are parts of supernova remnants. Smoker, Cox & Keenan (2011) find that in the IHVCs towards the LMC, Ca II is seen in 60 per cent of sightlines with only one tentative detection for Na I in a sample of 61 stars.

The RS effect is generally explained as follows (e.g. Vallerga et al. 1993). Sodium depletion is held to be more or less constant and small within the ISM (e.g. Welty, Morton & Hobbs 1996, and references therein), with virtually all interstellar calcium being contained within grains (Field 1974). If only some of the Ca is removed from grains, then the observed calcium gas-phase abundance should increase markedly as the Ca is returned to the gas phase. The most likely mechanism for grain destruction and subsequent return of Ca to the gas phase appears to be shocks. The velocity of the grains in the ISM is important as it has an effect on the speed of absorption from the gas phase on to the grains, and also desorption from the grains to the gas phase.

For the current sample there is one sightline for which we have a Ca II K detection and a Na I D non-detection which is the HVC towards the Cohen Stream (Cohen 1981) probed in Ca II K by Wakker et al. (2008) and in Na I with our FEROS data. The limit on the Na I/Ca II ratio is <0.36 dex for the Cohen Stream. This is typical for HVCs, many of which do not show any Na I absorption (Bekhti et al. 2008, and references therein).

For the IVC towards HD 93521 (IVA) the Na I/Ca II ratio is −0.25, which is in the range of values towards other IVCs (e.g. towards QSO B0515−4414; Bekhti et al. 2008) or towards local sightlines observed by Welsh et al. (2010) that have typical values from −0.3 to 1.3 dex.

Finally, towards QSO 0105+1619 (IVSouth) we have detections in the two species, with the Na I/Ca II ratio exceeding 1.5 dex. This is a much larger ratio than the other sightlines, although in the normal observed range.

Concluding, the IHVCs in the current sample follow the general trend of decreasing Na I/Ca II ratio with increasing LSR velocity, hence confirming the RS effect in intermediate- and high-velocity gas, although the scatter on the measurements is large.

4.5 The Ca II/H I ratio

Two of our sightlines have Ca II/H I measurements, with $\log A$ being -7.5 for IVA [probe star HD 93521 towards which $\log(N_{\rm H\,I}) = 19.70\,{\rm cm}^{-2}$] and -7.70 for IVSouth [QSO 0105+1619 probe towards which $\log(N_{\rm H\,I}) = 19.75\,{\rm cm}^{-2}$]. These values lie close to the best-fitting line of Wakker & Mathis (2000) and Smoker et al. (2003) and indicate the well-known trend by which the gas-phase abundance of Ca II decreases with increasing H I column density as ions are removed from the gas phase as they stick to dust grains.

4.6 Cloud physical conditions

In the data set of Welty et al. (1996), high-resolution (0.3–1.2 km s^{-1}) spectra were used to provide important constraints on the physical conditions within clouds. In particular, the comparison of b-values between two species of different atomic weights (Ca II and Na I) were used to differentiate thermal and turbulent broadening. This is because the b-value is related to the mass (m), temperature (T) and line-of-sight turbulent velocity dispersion $\sigma_{\rm t}$; thus, $b = [(2kT/m) + 2\sigma_{\rm t}^2]$ (Cowie & Songaila 1986), where k is Boltzmann constant. In particular, Welty et al. note that if Ca II and Na I D were similarly distributed, then $0.76 \leq b({\rm Ca\,II})/b({\rm Na\,I}) \leq 1.0$, with the lower and upper limits corresponding to purely thermal and turbulent broadening, respectively. In the absence of turbulent velocities, the temperature of a gas cloud can be derived from the above formula. Typical b-values in low-velocity gas are 1.3 km s^{-1} for Ca II K (Welty et al. 1996) and 0.7 km s^{-1} for Na I D (Welty, Hobbs & Kulkarni 1994).

Towards HD 93521 (Complex IVA) the Ca II and Na I data appear to have two components with velocity widths of 21 ± 4 and 6.7 ± 1.0 km s^{-1} (Ca II) and 12 ± 2 and 5.0 ± 5.0 km s^{-1} (Na I). Corrected for instrumental broadening of $\sim$7 km s^{-1} this leads to b-values for the components of 12 km s^{-1} (Ca II) and 5.9 km s^{-1} for the broad components, with the narrow Na I components being unresolved. These values lead in upper limits to the kinetic temperature exceeding 100 000 K. These temperatures are much too high for such singly ionized and neutral species and indicate either (1) high turbulent velocities and/or (2) multicomponent structure or problems resolving the individual components.

For QSO 0105+1619 ($R = 35\,000$) the FWHM observed in Ca II K and Na I D are 8.5 and 8.3 km s^{-1}, uncorrected for instrumental broadening. These are very similar to the instrumental resolution, and thus the true b-value and temperature for the IVC components cannot be derived with any certainty.

In conclusion, no accurate temperatures can be derived with the current spectra. Higher resolution observations would be useful for this and other sightlines to better investigate the physical conditions.

5 SUMMARY

Using a combination of archive and new echelle spectroscopic observations, we have observed sightlines towards a number of IHVCs with the intention of improving their distance estimates and determining their gas-phase abundances. The lack of Ca II K or Na I D absorption towards three stars in the lines of sight to IVCs and HVCs has improved the lower distance limits towards the ACS ($D > 8$ kpc) from probe star HDE 256725, Complex EP ($D > 7.6$ kpc) from probe star HD 86248 and Complex H ($D > 6.6$ kpc) from probe star HD 216411.

Na I/Ca II ratios towards the Cohen Stream HVC and IVA IVC were found to be <0.36 and -0.25 dex, which are indicative of the RS effect. Towards the QSO 0105+1619 (IVSouth) we have detections in the two species with Na I/Ca II ratio exceeding 1.5 dex, which although somewhat higher than the other two sightlines is within the normal range observed by Welsh et al. (2010).

Future work will include re-observation of the IHVCs detected in this paper at higher spectral resolution, and an investigation of the RS effect in data taken from the Paranal Observatory Project.

ACKNOWLEDGMENTS

We would like to thank the staff at La Silla for their expert help with the FEROS observations, in particular Oliver Schuetz. Data from ESO FEROS programme ID 078.C-0493(A) and FLAMES programme 171.D-0237(B) were taken from the ESO archive. FPK is grateful to AWE Aldermaston for the award of a William Penney Fellowship. This research has made use of the SIMBAD data base, operated at CDS, Strasbourg, France, the ELODIE archive at Observatoire de Haute-Provence (OHP), the Keck Observatory Archive (KOA), which is operated by the W. M. Keck Observatory and the NASA Exoplanet Science Institute (NExScI) under contract with the National Aeronautics and Space Administration, and the ESO Archive. JVS acknowledges financial support from Queen's University, Belfast and to Amazonas Inn, Quito, Ecuador and Hostal Gobernador, Arequipa, Peru for hospitality. JVS thanks the ESO Director General Discretionary Fund and Queen's University Belfast Visiting Scientist Fund for support. JVS thanks Alain Smette for providing wavelengths of telluric lines and an anonymous referee for many useful comments on the original version of this paper. This paper is dedicated to the memory of Jim Cohen.

REFERENCES

Bagnulo S., Jehin E., Ledoux C., Cabanac R., Melo C., Gilmozzi R., 2003, ESO Messenger, 114, 10
Bajaja E., Arnal E. M., Larrarte J. J., Morras R., Pöppel W. G. L., Kalberla P. M. W., 2005, A&A, 440, 767
Bekhti N. B., Richter P., Westmeier T., Murphy M. T., 2008, A&A, 487, 583
Blitz L., Spergel D. N., Teuben P. J., Hartmann D., Burton W. B., 1999, ApJ, 514, 818
Braun B., Burton W. B., 1999, A&A, 341, 437
Buenrostro V., Lockman J., Beckman J. E., 2008, in Knapen J. H., Mahoney T. J., Vazdekis A., eds, ASP Conf. Ser. Vol. 390, Pathways Through an Eclectic Universe. Astron. Soc. Pac., San Francisco, p. 384
Centurión M., Vladilo G., de Boer K. S., Herbstmeier U., Schwarz U. J., 1994, A&A, 292, 261
Cohen R. J., 1981, MNRAS, 196, 835
Cowie L. L., Songaila A., 1986, ARA&A, 24, 499
Danly L., 1989, ApJ, 342, 785
Danly L., Albert C. E., Kuntz K. D., 1993, ApJ, 299, 852
Dekker H., D'Odorico S., Kaufer A., Delabre B., Kotzlowski H., 2000, in Iye M., Moorwood A. F., M. eds, Proc. SPIE Vol. 4008, Optical and IR Telescope Instrumentation and Detectors. SPIE, Bellingham, p. 534
Diplas A., Savage B. D., 1994, ApJS, 93, 211
Ferlet R., Vidal-Madjar A., Gry C., 1985, ApJ, 298, 838
Field G. B., 1974, ApJ, 187, 453
Garmany C. D., Conti P. S., Massey P., 1987, AJ, 93, 1070
Giovanelli R., Haynes M. P., Kent B. R., Adams E. A. K., 2010, ApJ, 708, 22
Hartmann D., Burton W. B., 1997, Atlas of Galactic Neutral Hydrogen. Cambridge Univ. Press, Cambridge
Heiles C., 1984, ApJS, 55, 585

Howarth I. D., Price R. J., Crawford I. A., Hawkins I., 2002, MNRAS, 335, 267
Howarth I. D., Murray J., Mills D., Berry D. S., 2003, Starlink User Note SUN 50, Rutherford Appleton Laboratory/CCLRC
Hulsbosch A. N. M., 1978, A&A, 66, L5
Hunter I., Smoker J. V., Keenan F. P., Ledoux C., Jehin E., Cabanac R., Melo C., Bagnulo S., 2006, MNRAS, 367, 1478
Kalberla P. M. W., Burton W. B., Hartmann D., Arnal E. M., Bajaja E., Morras R., Pöppel W. G. L., 2005, A&A, 440, 775
Kaufer A., Stahl O., Tubbesing S., Norregaard P., Avila G., Francois P., Pasquini L., Pizzella A., 1999, The Messenger, 95, 8
Kulkarni S. R., Mathieu R., 1986, Ap&SS, 118, 531
Kuntz K. D., Danly L., 1996, ApJ, 457, 703
Lockman F. J., 2003, ApJ, 591, 33
Lockman F. J., Benjemin R. A., Heroux A. J., Lagnston G. I., 2008, ApJ, 679, 21
McClure-Griffiths N. M. et al., 2008, ApJ, 673, L143
Moore B., Ghigna S., Governato F., Lake G., Quinn T., Stadel J., Tozzi P., 1999, ApJ, 524, 19
Morton D. C., 2003, ApJS, 149, 205
Morton D. C., 2004, ApJS, 151, 403
Moultaka J., Ilovaisky S. A., Prugniel P., Soubiran C., 2004, PASP, 116, 693
Muller C. A., Oort J. H., Raimond E., 1963, C. R. Acad. Sci. Paris, 257, 1661
Pisano D. J., Barnes D. G., Gibson B. K., Staveley-Smith L., Freeman K. C., Kilborn V. A., 2004, ApJ, 610, L17
Putman M. et al., 2009, ApJ, 703, 1486
Riess A. G. et al., 2009, ApJ, 699, 539
Romano D., Tosi M., Chiappini C., Matteucci F., 2006, MNRAS, 369, 295
Routly P. M., Spitzer L., 1952, ApJ, 115, 227
Savage B. D., Wakker B. P., 2009, ApJ, 702, 1472
Savage B. D. et al., 2000, ApJ, 538, 27
Schmidt-Kaler Th., 1982, in Schaifers K., Voigt H. H., eds, Landolt-Boernstein, group VI, Subvol. b, Stars and Star Clusters, Vol. 2. Springer, Berlin, p. 17
Schwarz U. J., Wakker B. P., van Woerden H., 1995, A&A, 302, 364
Siluk R. S., Silk J., 1974, ApJ, 192, 51
Smoker J. V. et al., 2003, MNRAS, 346, 119
Smoker J. V., Lynn B. B., Christian D. J., Keenan F. P., 2006, MNRAS, 370, 151
Smoker J. V. et al., 2007, MNRAS, 378, 947
Smoker J. V., Cox A., Keenan F. P., 2011, MNRAS, submitted
Tamanaha C. M., 1994, ApJ, 433, 648
Tamanaha C. M., 1995, ApJ, 450, 638
Tamanaha C. M., 1996, ApJS, 104, 81
Tamanaha C. M., 1997, ApJS, 109, 139
Thom C., Putman M. E., Gibson B. K., Christlieb N., Flynn C., Beers T. C., Wilhelm R., Lee Y. S., 2006, ApJ, 638, L97
Thom C., Peek J. E. G., Putman M. E., Heiles Carl., Peek K. M. G., Wilhelm R., 2008, ApJ, 684, 364
Vacca W. D., Garmany C. D., Shull J. M., 1996, ApJ, 460, 914
Vallerga J. V., Vedder P. W., Craig N., Welsh B. Y., 1993, ApJ, 411, 729
van Kuilenburg J., 1972, A&AS, 5, 1
van Woerden H., Schwarz U. J., Peletier R. F., Wakker B. P., Kalberla P. M. W., 1999, Nat, 400, 138
Vogt S. S. et al., 1994, in Crawford D. L., Craine E. R., eds, Proc. SPIE Vol. 2198, Instrumentation in Astronomy VIII. SPIE, Bellingham, p. 362
Wakker B. P., 1991, A&A, 250, 499
Wakker B. P., 2001, ApJS, 136, 463
Wakker B. P., Mathis J. S., 2000, ApJ, 544, 107
Wakker B. P., van Woerden H., 1991, A&A, 250, 509
Wakker B. P., van Woerden H., 1997, ARA&A, 35, 217
Wakker B. P., Kalberla P. M. W., van Woerden H., de Boer K. S., Putman M. E., 2001, ApJS, 136, 537
Wakker B. P. et al., 2007, ApJ, 670, 113
Wakker B. P., York D. G., Wilhelm R., Barentine J. C., Richter P., Beers T. C., Ivezic Z., Howk J. C., 2008, ApJ, 672, 298
Wallace P., Clayton C., 1996, rv, Starlink User Note SUN 78, Rutherford Appleton Laboratory/CCLRC
Wegner W., 1994, MNRAS, 270, 229
Wegner W., 2000, MNRAS, 319, 771
Welsh B. Y., Lallement R., Vergely J.-L., Raimond S., 2010, A&A, 510, 54
Welty D. E., Hobbs L. M., Kulkarni V. P., 1994, ApJ, 436, 152
Welty D. E., Morton D. C., Hobbs L. M., 1996, ApJS, 106, 533
Wesselius P. R., Fejes I., 1973, A&A, 24, 15
Westmeier T., Braun R., Thilker D., 2005, A&A, 436, 101
Westmeier T., Brüns C., Kerp J., Thilker D. A., 2007, New Astron. Rev., 51, 108
Westmeier T., Brüns C., Kerp J., 2008, MNRAS, 390, 1691

SUPPORTING INFORMATION

Additional Supporting Information may be found in the online version of this article:

Table 3. The sample of objects.
Fig. A1. Optical Ti II, Ca II K, Na I D and K I normalized spectra taken from the FEROS, UVES, ELODIE and HIRES archives plus 21-cm H I spectra taken from the LABS survey data.

Please note: Wiley-Blackwell are not responsible for the content or functionality of any supporting materials supplied by the authors. Any queries (other than missing material) should be directed to the corresponding author for the article.

This paper has been typeset from a TEX/LATEX file prepared by the author.